Clays and Clay Minerals, Vol. 47, No. 4, 495–504, 1999.

PREFERRED ORIENTATION OF PHYLLOSILICATES IN GULF COAST MUDSTONES AND RELATION TO THE SMECTITE-ILLITE TRANSITION

NEI-CHE HO, DONALD R. PEACOR, AND BEN A. VAN DER PLUIJM

Department of Geological Sciences, The University of Michigan, 2534 C.C. Little Building, Ann Arbor, Michigan 48109-1063, USA

Abstract—Development of preferred orientations of illite-smectite (I-S) has been studied using X-ray diffraction (XRD) texture goniometry to produce pole figures for clay minerals of a suite of 16 mudstone samples from a core from the Gulf Coast. Samples represent a compaction-loading environment in which the smectite-to-illite (S-I) transition occurs. In five shallow, pre-transition samples, there is no significant preferred orientation for smectite-rich I-S. Development of preferred orientation of I-S, although weak, was first detected at depths slightly less than that of the S-I transition. The degree of preferred orientation, which is always bedding-parallel, increases rather abruptly, but continuously, over a narrow interval corresponding to the onset of the S-I transition, then continues to strengthen only slightly with increasing depth. The degree of post-transition preferred orientation is also dependent on lithology, where the preferred orientation is less well-defined for quartz-rich samples.

Previously obtained transmission electron microscope (TEM) data define textures consistent with the change in orientation over many crystallites. The smectite in pre-transition rocks consists largely of anastomosing, "wavy" layers with variable orientation and whose mean orientation is parallel to bedding, but which deviate continuously from that orientation. This results in broad, poorly defined peaks in pole figures. Post-transition illite, by contrast, consists of thin, straight packets, with most individual crystallites being parallel or nearly parallel to bedding. This results in pole figures with sharply defined maxima. By analogy with development of slaty cleavage in response to tectonic stress during metamorphism, the S-I transition is marked by dissolution of smectite and neocrystallization of illite or I-S locally within the continuous "megacrystals" of smectite. The transition is inferred to have some component of mechanical rotation of coherent illite crystals within a pliant matrix of smectite. The data suggest that change in orientation and coalescence of clay packets plays an important role in the formation of the hydraulic seal required for overpressure generation.

Key Words—Gulf Coast, Phyllosilicates, Preferred Orientation, Smectite-Illite Transition.

INTRODUCTION

The sequence of changes in Gulf Coast mudstones as a function of increasing depth has been extensively studied and serves as a "type" sequence, in part because of its significance as a source of hydrocarbons. A critical component of the sequence is the transformation of smectite to illite (S-I); the mineralogical relations of the transformation were defined in the classic study of Hower *et al.* (1976). This transformation approximately parallels maturation of hydrocarbons, and probably plays a critical role in fluid migration (*e.g.*, Burst, 1969).

Porosity and permeability are parameters critical to water-mineral interactions and fluid (water or hydrocarbon) migration. In pelites undergoing diagenesis in a passive, tectonic-stress-free environment, these properties are mostly determined by smectite that remains largely unchanged preceeding the transformation from smectite to illite, and then by illite that changes little subsequent to that transition. Most of the water originally present in unconsolidated sediments is lost during early compaction with only a small, continuous decrease with increasing depth (*e.g.*, Powers, 1967). At depths of ~1000 m, pore water cannot be further removed from pelitic sediments by compaction; porosity and permeability are therefore essentially eliminated before sediments reach the thermal hydrocarbon generation window (Bruce, 1984). A second source of water is the interlayer water in smectite, some of which may be released as pore water at depths above and at the S-I transition (Colten-Bradley, 1987). Powers (1967) proposed a two-stage fluid-release process, suggesting that the S-I transition is the source of the second release of fluid that serves as the vehicle for hydrocarbon migration. Although this two-stage mechanism was later refined by Burst (1969) into a three-stage system, the S-I transition is closely related to hydrocarbon maturation and the evolved water aids hydrocarbon migration.

Although fluid flow may occur with normal fluid pressures, abnormally high fluid pressure, or overpressure, results in pressure gradients that lead to fluid flow (Bruce, 1984). At a given depth, if hydraulic continuity between fluid in the rock and the surface is maintained, the fluid pressure equals the load of a water column extending from the surface to that depth (hydrostatic pressure). The effective pressure at that depth is the portion of the total vertical stress supported by grain-grain contacts of the sediment particles, and it is the difference between the total overburden pressure and the fluid pressure (Plumley,

1980). Overpressure is present when the fluid pressure is greater than hydrostatic pressure, a condition common in Gulf Coast sediments. Many mechanisms have been proposed as sources of overpressure, including: 1) compaction disequilibrium (*e.g.*, Magara, 1975a; Chapman, 1980; Mello and Karner, 1996), 2) aquathermal pressure (*e.g.*, Barker, 1972; Magara, 1975b; Sharp, 1983; Luo *et al.*, 1994), and 3) clay transformation (*e.g.*, Powers, 1967; Plumley, 1980; Bruce, 1984; Pendkar and Jordan, 1993; Luo *et al.*, 1994). Regardless of the mechanism, all require reduction in porosity and permeability, and most importantly, a sealing mechanism that isolates the pore water from the surface (*e.g.*, Mello *et al.*, 1994). Although it has been suggested that the S-I transformation may not solely account for the presence of high pore fluid pressures (*e.g.*, Chapman, 1980), transmission electron microscopy (TEM) studies in Gulf Coast mudstones (Freed and Peacor, 1989a) and North Sea siltstones (Nadeau, pers. comm.) showed that there is a dramatic change in texture concomitant with the S-I transformation, and that such changes are at least compatible with a sealing effect.

Because of its association with hydrocarbon generation and migration, much research has focused on the S-I transition process using techniques such as powder X-ray diffraction (XRD) (*e.g.*, Srodon, 1980; Reynolds, 1992), TEM (*e.g.*, Ahn and Peacor, 1986; Jiang *et al.*, 1990; Guthrie and Veblen, 1989), and nuclear magnetic resonance (NMR) spectroscopy (*e.g.*, Barron *et al.*, 1985). Mineralogical relations were summarized by Hower *et al.* (1976). It is generally agreed that clay in mudstones consists of (Reichweite) R0 I-S with ~20% illite at all depths extending to the onset of the S-I transition. That transition then occurs over a relatively narrow range of depths. Clay minerals remain largely unchanged with further depth, consisting of ~80% illite in I-S according to XRD data. The S-I transformation involves release of interlayer water, substitution of Al^{3+} for Si^{4+} and fixation of K^+, which is approximated by the reaction (Hower *et al.*, 1976): smectite + Al^{3+} + K^+ = illite + Si^{4+}. This process is independent of formation boundaries, depth, and geological age (*e.g.*, Bruce, 1984). Rather, temperature is generally inferred to be the variable most affecting reaction progress (Perry and Hower, 1970). Several transformation mechanisms have been proposed, and the subject remains controversial (*e.g.*, Altaner and Ylagen, 1997). For example, Hower *et al.* (1976) implied a process of progressive replacement of layers of smectite by layers of illite, whereas Pevear and Reynolds (1997) proposed precipitation of illite on a substrate of detrital mica. Ahn and Peacor (1986) proposed a model involving local dissolution of smectite and precipitation of illite. The specifics of the reaction process are subject to debate, but it is generally agreed that layers of illite retain at least the approximate orientations of preexisting layers of smectite as demonstrated by TEM images.

Much research on rocks bearing I-S has focused independently on the mineralogical relations and physical properties such as porosity and permeability. These properties must clearly be related to the mineralogy, crystallite size, and spatial orientations of the clay minerals. The changes in texture concomitant with the transition as documented by Freed and Peacor (1989a) may be accompanied by changes in preferred orientation of the clays that are a critical component of changes in porosity and permeability. Despite the probability of a link between the latter properties, mineralogical changes, and preferred orientation, there are few studies that give quantitative data regarding the degree of preferred orientation and its variation as a function of depth (*e.g.*, Sintubin, 1994), and none in relation to the S-I transformation.

Several methods exist for the quantitative determination of preferred orientation, but the most direct involves XRD. Automated instrumentation and software were developed in our laboratory to produce contoured pole figures showing the preferred orientation of phyllosilicates; procedures, equipment design, and treatment of data are found in van der Pluijm *et al.* (1994, 1995). We refer to our method as high-resolution X-ray texture goniometry (HRXTG) because it utilizes the narrow collimated X-ray beam of a single-crystal diffractometer to interact with a small sample area, rather than the broad divergent beam of a powder diffractometer. The sequence of pelites in the Gulf Coast has been affected only by burial stresses and not by tectonic stress. The sequence progresses as a continuous function of depth interrupted only by the S-I transformation, which has important consequences for porosity and permeability, overpressure, and fluid migration. The samples were previously studied by other methods, including TEM (*e.g.*, Dong and Peacor, 1996; Dong *et al.*, 1997) so that XRD preferred-orientation data can be linked with mineralogical relations and detailed textures in high-resolution images. These relations in turn can be used for the interpretation of higher grade processes which are related to modification of burial metamorphic textures, such as slaty-cleavage development.

SAMPLE DESCRIPTIONS

Mudstone samples were originally obtained from the Socony Mobil Oil Company No. 1 Zula E. Boyd well, DeWitt County, Texas, drilled to a depth of 4300 m. The well first penetrated the near-surface Miocene Fleming Formation and then a thick Tertiary section, intersecting Cretaceous sediments at ~3370 m. This sequence represents a passive margin deposition environment, with at least a mud-dominated progradational system in the Late Cretaceous, a regressive event in the Tertiary, three major regressive-transgres-

Table 1. Summary of sample data. Because samples are in the form of cuttings, the depths are given as intervals of 9 m. Illite content, if available, and additional data such as core temperatures, were given by Freed and Peacor (1992). Data shown in Figures 1 and 2 are denoted with "2". Samples 1–6 are pre-S-I transitional, 7–9 are transitional, and 10–16 are post-transitional. n/a (not applicable) refers to I-S peaks that are so broad that no single peak 2θ-value is evident, and/or to the lack of an identifiable pole density maximum.

ID	Depth (m)	% Illite[1]	D_{mix} (Å)	Max. pole density (mrd)		Max. contour (mrd)	Contour interval (mrd)
				D_{10}	D_{mix}		
1	64–73	—	n/a	1.76[2]	n/a	1.70	0.2
2	300–309	42	n/a	1.77[2]	n/a	1.70	0.2
3	610–618	30	n/a	2.94[2]	n/a	2.80	0.5
4	748–758	—	12.4	1.75[2]	n/a	1.70	0.2
5	912–921	32	n/a	1.71[2]	n/a	1.70	0.2
6	1812–1821	35	12.5	3.57	3.06[2]	3.00	0.5
7	1967–1976	—	11.9	6.43	5.28[2]	5.20	0.5
8	2267–2276	50	12.5	5.97	5.77[2]	5.70	0.5
9	2421–2430	87	12.5	4.51	3.08[2]	3.00	0.5
10	2876–2885	80	11.0	6.03	5.95[2]	5.90	0.5
11	3024–3033	77	10.7	3.39	3.42[2]	3.40	0.5
12	3479–3488	89	10.9	7.01	6.42[2]	6.40	0.5
13	3633–3642	88	11.0	4.81	4.30[2]	4.30	0.5
14	3788–3797	—	10.7	6.75	6.29[2]	6.20	0.5
15	4085–4094	—	10.9	3.58	3.52[2]	3.50	0.5
16	4242–4245	—	10.9	3.34	3.16[2]	3.10	0.5

[1] Freed and Peacor (1992).
[2] Data shown in Figure 2.

sive cycles in the Eocene, and a final regression in the Oligocene (Freed and Peacor, 1992). There is no report of abnormal fluid pressures encountered during drilling.

These samples were chosen because of previous detailed characterization using XRD (Freed and Peacor, 1987, 1992) and TEM (Freed and Peacor, 1987, 1989b, 1992; Dong and Peacor, 1996; Dong *et al.*, 1997). Those TEM observations provided direct visualization of the textural relationships reflected in HRXTG data, and of the kind of S-I transition specific to the studied samples. A total of 16 clay-rich pelites were obtained from depths of ~60 to 4250 m, numbered sequentially with increasing depth. Table 1 summarizes the depth of each sample and the illite-smectite content (in % illite) where determined by Freed and Peacor (1992). Because these samples are cuttings from cores, the depths are given as intervals of ~9 m. Specific cuttings were chosen where bedding directions could be recognized by features such as color variation and preferred breakage, as subsequently verified by TEM images of preferred grain orientations.

According to Freed and Peacor (1992), S-I transitional samples occur between depths of ~2100 m (83°C) and ~2400 m (88°C), corresponding approximately to samples 7–9 of this study. Samples from the pre-transition zone are smectite-rich; XRD data (Freed and Peacor, 1992) indicate ~35% illite in R0 mixed-layered I-S in the pre-transition zone samples. The illite content increases abruptly to ~85% across the transition, then remains nearly constant for deeper samples. TEM data confirmed that smectite is the dominant authigenic phase in shallow samples. As the S-I transition proceeds, subhedral crystals of R1 I-S and subsequently illite were observed within a framework of smectite, with their proportion increasing relative to smectite with increasing depth until virtually all smectite was replaced by illite crystallites averaging ~100 Å in thickness.

ANALYTICAL TECHNIQUES AND SAMPLE PREPARATION

The HRXTG device is an attachment to an automated Enraf-Nonius CAD4 single-crystal diffractometer with a MoKα-radiation source and scintillation detector. Preferred-orientation data were measured in transmission mode, which is recommended for XRD peaks with low diffraction angles (2θ) such as for the relatively intense (001) peaks of phyllosilicates (*e.g.*, Oertel, 1985; Wenk, 1985). In transmission mode, X-rays pass through the sample and the detector is positioned at a pre-set 2θ angle to receive X-rays diffracted by a specific set of planes of a specific phase. To measure the diffracted X-ray intensities in different orientations, the sample is rotated using the axial system of the CAD4 diffractometer and the pole-figure device to sample a grid of orientations, while the X-ray source and the detector remain stationary. At each orientation, both the diffracted intensity and the corresponding orientation information are recorded. Intensities are first corrected for background and absorption, then normalized so that the results are concentration-independent. The resulting values are relative pole densities, and are expressed in multiples of random

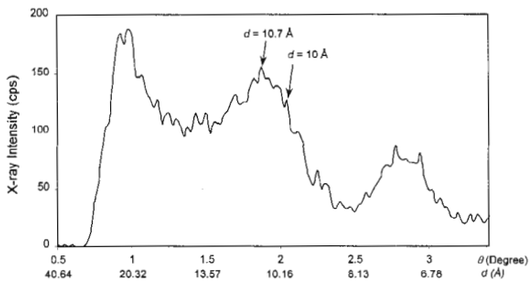

Figure 1. XRD pattern (2θ-scan) for sample 12 obtained with the single-crystal diffraction system is typical of this study. The 2θ values for D_{10} and D_{mix} are shown.

distribution (mrd; Wenk, 1985); *i.e.*, density of a given pole is calculated relative to the average pole density, which is determined by distributing the integrated total pole density uniformly over the full sphere. The final output is a contoured projection showing orientations of a given pole of a given set of planes (usually (001) in the case of phyllosilicates), plotted in lower-hemisphere equal-area projection. For details regarding instrumentation and correction procedures, see van der Pluijm *et al.* (1994). Measurements of most samples were carried out more than once to confirm the results.

Prior to the measurement of preferred-orientation data, a scan over a range of 2θ was made to: 1) validate phases present, based on previous determinations by standard powder XRD techniques, and determine the precise diffraction angles for data collection, and 2) determine an appropriate level of background correction. This kind of scan is called a "2θ-scan" to distinguish it from a "pole-figure scan" which generates preferred-orientation data. The 2θ-scan is essentially the same as a standard powder XRD pattern.

The specimens used for preferred orientation measurements are rock slices mounted on a square aluminum holder with a circular opening in its center to allow X-rays to pass. Rock slices are ~0.2 mm thick, and were cut perpendicular to bedding, as TEM observations (Dong and Peacor, 1996) confirmed preference for orientation of clay minerals parallel to bedding. The precise thickness of each specimen was measured to correct diffraction intensities for absorption. All samples, which consisted of small cuttings, were embedded in epoxy blocks before cutting so that the cross-section of the sample would be sufficiently large to fit the HRXTG sample holder. Smectite-rich samples, whose textures may have been affected by water during the sample preparation process, were first impregnated using epoxy resin to prevent expansion of smectite and resulting destruction of samples. To prevent sample deformation, impregnation was accomplished passively at room pressure. Similar treatment of samples studied by TEM verified the lack of deformation.

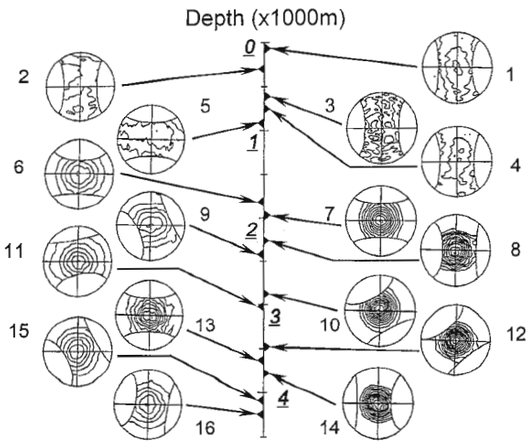

Figure 2. Pole figures. Those for samples 1–5 correspond to D_{10} and those for samples 6–16 to D_{mix}. Maximum contours and contour intervals are given in Table 1. The peak of the pole density distribution was rotated to the center of each plot for pole figures with well-defined maxima; this direction is within 10° of the normal to bedding. For shallow samples where there is no well-defined maximum, the estimate of the position of the pole normal to beddiug was rotated to the figure center. The shaded area represents the S-I transition zone. Pole figures are placed to the right or left of the depth indicator to conserve space.

RESULTS

A typical 2θ-scan is shown in Figure 1. The scans have a broad, intense peak with interplanar spacing between $d \sim 10$–14 Å, corresponding to mixed-layer I-S, and often a small, relatively sharp peak with $d \sim 10$ Å (not present in Figure 1), corresponding in part to detrital illite or muscovite (see below). Pole-figure scans were obtained at two values of 2θ for each sample, each measured twice. One was obtained for 2θ corresponding to $d \sim 10$ Å, a value that was constant for all samples. This position, corresponding to illite or muscovite, is referred to as D_{10} and largely represents the preferred orientation of detrital illite, if any, in pre-transition samples. The second 2θ value corresponded to the position of the maximum intensity of the broad peak between $d \sim 10$–14 Å; this position is designated as D_{mix}. The value of D_{mix} varied from sample to sample as a function of relative proportions of illite and smectite in I-S.

The maximum pole densities of all pole figures of both sets of data (for D_{10} and D_{mix}) are listed in Table 1. The normalized maximum pole density for samples without preferred orientation should be equal to a mrd of unity. However, in the case of an incomplete pole figure, *i.e.*, one for which data are available for less than a complete sphere as illustrated in Figure 2, the normalized maximum intensity for a random distribution is greater than one mrd because the X-ray intensities are normalized over a smaller area (approxi-

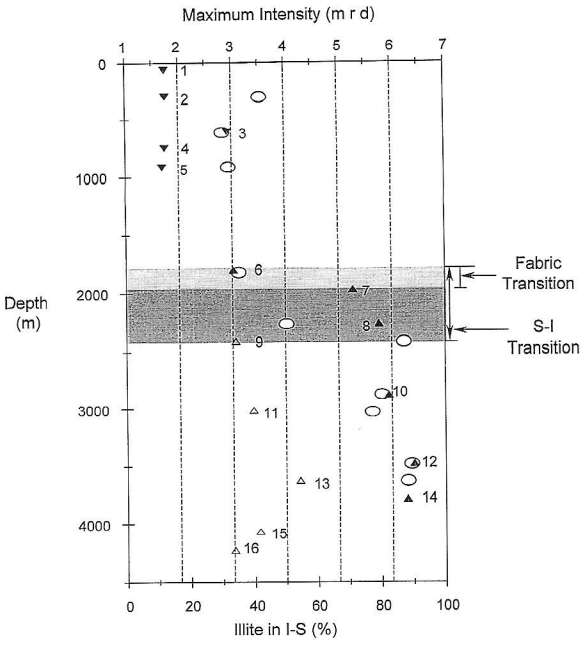

Figure 3. Maximum pole-figure densities and % illite in mixed-layer I-S. The shaded area represents the S-I transition zone. The values listed for "illite" correspond primarily to detrital grains (muscovite and illite) with $d \sim 10$ Å, whereas "I-S" corresponds principally to authigenic, illite-rich I-S. The designation I-S (sandy) corresponds to samples with relatively larger concentrations of detrital quartz grains. ○: % Illite, ▼: Illite, ▲: I-S, △: I-S (Sandy).

mately three quarters that of a complete pole figure). Nevertheless, since the same normalization procedure was applied to all samples, the results are internally consistent.

Selected pole figures are shown in Figure 2. D_{mix} pole figures for samples 1–5 are not illustrated as they showed no or weak preferred orientation and were based on poorly defined peaks in 2θ-scans; for samples 6–16, pole figures are given for D_{mix}. The D_{10} pole figures are omitted for samples 6–16 as they effectively duplicate those for D_{mix}. Maximum pole densities are plotted against depth in Figure 3. The maximum contours and the intervals used in each plot are also summarized in Table 1. Where contours are well defined, each pole figure was rotated so that the maximum pole density is at the center of the figure. In all cases, this direction is estimated to be within 10° of the normal to bedding, as determined by textural features of individual cuttings. The shaded areas in the middle of Figures 2 and 3 represent the S-I transition zone. All pole figures were processed through two smoothing cycles and rotated so that the maxima are oriented at the center of the plot (which also represents the approximate direction of the bedding pole). The rotation was performed to allow all plots to refer to the same orientation.

The first noticeable change is in the values of D_{mix}. For samples where viable data were determined, the values of D_{mix} for samples from both before and within the transition zone (samples 4 and 6–9) are relatively constant and ~12.5 Å, corresponding to smectite-rich I-S. The value of D_{mix} decreases abruptly, starting with sample 10. For the remaining post-transition zone samples (11–16), D_{mix} is ~11 Å with minor variations between samples. These values are consistent with those obtained using standard powder diffraction methods on such samples (*e.g.*, Hower *et al.*, 1976; Velde *et al.*, 1986).

Although the pole figures obtained for samples 1–5 using D_{mix} show no to very weak patterns, measurements using D_{10} for these samples showed weak preferred orientation. The maximum pole figure densities from D_{10} for samples 1, 2, 4, and 5 are approximately the same and relatively small compared to the measurements from the other samples. Sample 3 is an exception in that it has a relatively large maximum pole density.

For samples from depths greater than that for sample 5, D_{10} and D_{mix} pole figures are similar in orientation (always parallel to bedding). The maximum X-ray intensities generally increase with depth (Table 1; Figure 3), although with significant variation, the maximum densities of D_{mix}-pole figures are consistently equal to or slightly less than those of D_{10} for a given sample.

The maximum pole figure densities (from both D_{mix}- and D_{10}-pole figures) for samples from depths greater than that of sample 5 fall into two groups. One group has densities of ~3.5 mrd, including samples 6, 9, 11, 13, 15, and 16. The other group has relatively high densities of ~6 mrd, including samples 7, 8, 10, 12, and 14. The high- and low-density values occur in alternate samples, but that is apparently merely a matter of chance.

Samples from depths more shallow than that of sample 5 have pole-figure patterns that are very distinct from those of deeper samples. For these samples, the pole figures correspond to either a near-random pattern or a vaguely defined ellipsoid. In contrast, regardless of the pole figure densities, samples from greater depths all display well-defined circular patterns with a maximum density parallel to bedding. Although the maximum density of sample 3 is comparable to those of deeper samples, the full pole figure does not display any pattern.

DISCUSSION

Preferred orientation development

For those samples for which pole figures with well-defined maxima were obtained for both D_{mix} and D_{10}, the figures were quite similar so only those for D_{10} are shown in Figure 2. The similarity is in part an artifact

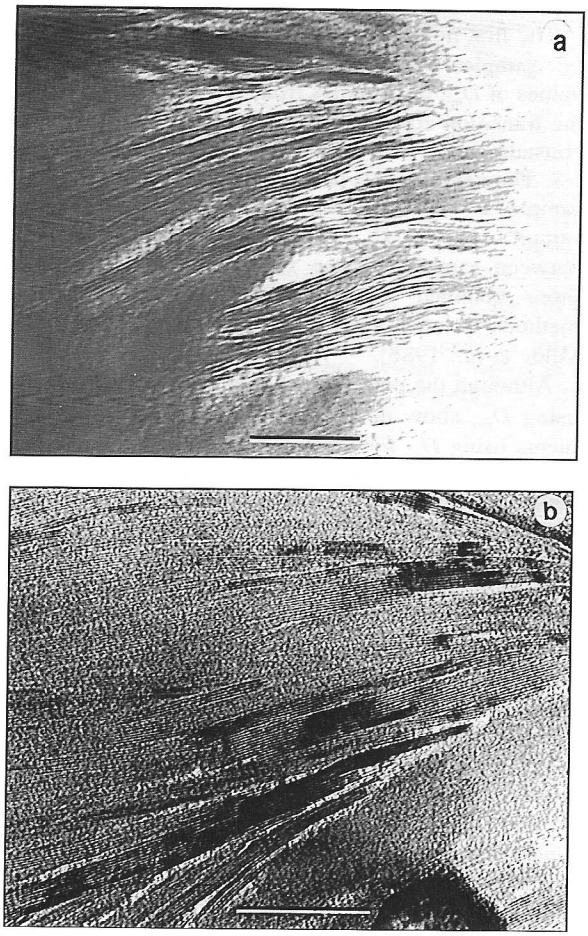

Figure 4. a) TEM image of smectite from a pre-transition zone sample and b) TEM image of illite from a post-transition zone sample. Scale bar is 0.05 μm. (images courtesy of H. Dong).

of the diffraction method; peaks are considerably broadened as a function of 2θ on the single-crystal diffractometer relative to those of a powder diffractometer, as a result of a collimated beam of X-rays rather than the parafocusing geometry of a powder diffractometer. The peak corresponding to D_{mix} is severely broadened on the scale of 2θ due to mixed-layering; this results in a contribution of diffraction of I-S to the peak at the fixed position of the relatively sharp peak corresponding to D_{10}. The pole figure for D_{10} otherwise would correspond only to detrital illite or muscovite in shallow samples, but therefore also has a contribution from smectite-rich I-S. Starting with the S-I transformation, the D_{mix} peak shifts progressively toward that for D_{10}. The overlap therefore becomes progressively greater, perhaps even dominating the contribution from detrital illite or muscovite in post-transition samples, thus explaining the similarity in pairs of pole figures for deep samples. The numerical values in given in Figures 2 and 3, therefore, only correspond to values of D_{mix} for samples 6–16.

In most pre-transition zone samples (samples 1–6), however, pole figures obtained using D_{mix} show no preferred orientations whereas those from D_{10} show weakly defined preferred orientation; *i.e.*, a broad peak of low intensity symmetrical about the pole to bedding. This is especially evident for the pole figures of samples 1 and 4 (Figure 2). There are two possible explanations for such low maxima: 1) Mineral (smectite) contents in the samples are too low. However, bulk powder XRD patterns and 2θ-scans for the same samples show that the dominant phase is smectite-rich R0 I-S, and thus mineral content can not be too small. 2) Minerals have no (or very weak) preferred orientations. TEM observations from pre-transition samples (*e.g.*, Ahn and Peacor, 1986; Dong *et al.*, 1997) showed that the smectite normally occurs in "megacrystals" (*e.g.*, Ahn and Peacor, 1986, their Figure 4). Thus individual layers of smectite are more or less continuous, but with common layer terminations and with orientations that vary continuously along a layer. TEM lattice-fringe images show that individual layers can be traced with parallel to subparallel contiguous layers over long distances, but with orientations changing over large angular ranges. A given layer may terminate but the adjacent layers continue, thus creating a continuous, but highly imperfect "megacrystal" which envelops the small proportion of detrital grains such as quartz. However, the orientation of layers is deflected in the vicinity of quartz grains to conform to that of the shape of such detrital grains, and the orientation becomes more variable with respect to bedding. Nevertheless, lattice-fringe images of smectite do indeed show a tendency for the wavy layers to be subparallel to bedding (Figure 4a). Such variable orientation is in sharp contrast to that shown in TEM images of post-transition illite, where illite occurs as packets of straight, relatively defect-free 10-Å layers (illustrated in Figure 4b and discussed below). We therefore conclude that the lack of detection of strong preferred orientation in the D_{mix}-pole figures of pre-transition samples is a reflection of the continuous variation in the orientation of smectite layers over a wide range of orientations, albeit with an average orientation equal to or near that of bedding.

The D_{10}-pole figures for the pre-transition samples (samples 1–6) show very weakly defined preferred orientation parallel to bedding. TEM observations generally show that flattened detrital phyllosilicate grains are aligned parallel or subparallel to enclosing smectite. To a first approximation, then, the preferred orientation of detrital illite or muscovite would be expected to be the same as that of smectite. The relative perfection of detrital phyllosilicates, leading to sharp peaks, is in sharp contrast with the highly imperfect array of smectite layers that lead to broadening of X-

ray peaks. We ascribe the lack of any preferred orientation in the D_{mix}-pole figures to a combination of very weakly defined preferred orientation and broadened diffraction maxima. Figures 2 and 3 therefore include data only for D_{10}-pole figures in pre-transition samples, those for D_{mix} being featureless.

In the post-transition zone samples, all the pole figures show similar circular patterns. Such circular patterns are typical of a compaction environment where layer-parallel tectonic stresses were absent. The maximum densities of the D_{mix}-pole figures fall into two distinct groups. One group of samples has "high" densities of ~6 mrd, and the other "low" densities of ~3.5 mrd. We ascribe these differences in strength of preferred orientation to the presence of detrital grains. Powder XRD patterns of all post-transition samples fall into two distinct groups corresponding exactly to those for pole-figure density. The powder XRD data show that the proportion of quartz, which is primarily of detrital origin, is significantly higher in the samples with low densities, by factors to two. Van der Pluijm *et al.* (1994) showed that the pole-figure peak density decreased in direct proportion to an increasing ratio of quartz to clay contents, in a 2-cm thick sediment sequence in which the proportion of quartz varies strongly. The increased quartz content causes phyllosilicate grains to have orientations conforming to detrital grain shapes and therefore to be more random. This, in fact, is similar to a well-known experimental technique of minimizing preferred orientation of clay minerals in X-ray diffractometer patterns by spiking samples with materials such as crushed glass.

S-I transition and preferred orientation

The overall trend in preferred orientation is one in which pre-transition samples have a near-constant, but weak preferred orientation, whereas post-transition samples have strong, well-developed preferred orientations, with a rapid change at approximately the onset of the S-I transition. This suggests that the S-I transition is intimately related to the development of the strong preferred orientation.

Freed and Peacor (1989a) compared the textures of pre-transition smectite-rich and post-transition illite-rich mudstones from the Gulf Coast, and concluded that, in addition to the release of interlayer water as pore fluid, the S-I transition facilitates the generation of overpressure by providing an effective hydraulic seal. Figure 4b shows the texture typical of illite-rich mudstones, which contrasts sharply with that of the smectite-rich mudstones of Figure 4a. Rather than consisting of a continuous, anastomosing array of layers as in smectite, illite occurs as discrete packets of straight, relatively defect-free layers that comprise individual crystallites; their mean thickness is on the order of 100 Å as directly measured from the TEM images of Ahn and Peacor (1986), Freed and Peacor (1989a), and Dong *et al.* (1997) by R. J. Merriman (pers. comm.). Such discrete crystals sometimes form stacks in which individual discrete packets are subparallel, somewhat like the cards in a badly stacked deck. Packets thus form an array whereby there is very limited pore space at packet contacts. No pore space was resolvable in SEM images of samples of this study. It is even difficult to detect pore space having dimensions as large as tens of angstroms in the highest resolution TEM images. However, especially where packets intersect at low angles, pore space may be observed that is on the order of only a few angstroms in maximum dimension. More importantly, such pore space is always defined by localized grain-grain contacts, and always appears to be discrete and disconnected; *i.e.*, the pore space appears to be consistent with vanishingly small permeability. However, it is noteworthy that observations are made after removing the sample from a fluid-rich environment under pressure, whereas the samples are under vacuum when studied by electron microscopy. Pore space may be diminished by the change in environment. Alternatively, contraction of shale samples during loss of water is normally accompanied by strain features (*e.g.*, as exemplified by lens-like openings in dehydrated smectite). Lack of detectable porosity described herein, however, is for samples which display no strain features.

TEM images show a dramatically different texture in illite-rich mudstones, where packets appear to have a much higher portion of layers (sub)parallel to bedding, as compared with smectite. Such relations are therefore consistent with the sharp increase in degree of preferred orientation during the S-I transformation. The abrupt changes in preferred orientation, clay mineral assemblage, textures of the clay minerals, and the occurrence of overpressure as reported in other cores in the Gulf Coast sediments, all occur in a near parallel fashion, and comprise a consistent set of diverse data. The mechanism of transformation of smectite to illite is controversial, perhaps occurring in different sediment sequences by mechanisms as diverse as layer-by-layer replacement or complete dissolution and neocrystallization. As directly observed by TEM methods for the specific samples used in this study, however, the transition occurs by local dissolution of smectite with neocrystallization of discrete, subhedral crystals of R1 I-S or illite within the enclosing smectite matrix (Ahn and Peacor, 1986; Freed and Peacor, 1992; Dong *et al.*, 1997). Such subhedral crystals retain the approximate orientation of precursor smectite layers, and gradually increase in size, consuming the smectite, until they coalesce to form the pore-space-free (and presumably, the relatively impermeable) array of interlocking illite crystals. Such growing, coherent crystals are immersed in anastomosing smectite layers, allowing them to respond to load stress, with their orienta-

tions adjusting gradually by rotation to the plane of bedding. The smectite-rich samples thus give rise to continuously variable pole figure orientations over a broad angular range and with a poorly defined maximum, whereas illite-rich samples result in a narrow range of orientations having a well-defined maximum pole density.

Changes in preferred orientation are analogous to the development of slaty cleavage in response to tectonic stress, where mineral-grain orientation changes from bedding-parallel to cleavage-parallel. The debate about a mechanism has long centered on mechanical rotation of phyllosilicate grains or dissolution-neocrystallization, van der Pluijm *et al.* (1998) having shown that both mechanisms may be active under some conditions. For the S-I transformation, the process is dissolution of smectite and neocrystallization of illite or R1 I-S normal to load stress, which is thus analogous to dissolution of clay minerals parallel to bedding and neocrystallization of mica normal to principal tectonic stress. Thus, the relatively defect-free, growing coherent illite crystallites can rotate within the enclosing incoherent array of smectite. Therefore, increase in preferred orientation has elements both of dissolution-neocrystallization and grain rotation.

Relation of preferred orientation data to porosity, permeability, and geopressuring

We do not establish the relation between preferred orientation and properties such as porosity and permeability, but we do make quantitative measures relating to orientation in clay minerals in a typical mudstone sequence. Nevertheless, changes in preferred orientation concomitant with the I-S transition must reflect differences in texture. In addition there is a clear relationship between the I-S transition and geopressuring in some sediment sequences (see below), further linking the change in preferred orientation to porosity and permeability. Because porosity and permeability are controlled by textural relations, all of these variables must be linked in some way.

Direct measurements for shales show a continuous decrease in porosity as a function of depth with little or no change associated with the S-I transition. For example, Maxwell (1964) showed for his shales that porosity decreased rapidly at relatively shallow depths, but stabilized at ~1200 m. Porosity actually increased very slightly at a depth of ~2400 m, which is approximately where the S-I transition occurs, but the change was subtle. Plumley (1980) showed, using γ-γ density logs for Gulf Coast sediments, that there is a continuous decrease in porosity to the depth of the onset of the S-I transition. With further increase in depth, porosity is constant or slightly larger. Similar results showing continuous increases in porosity as a function of depth, with no discontinuities associated with the S-I transition, have been reported by many investigators (*e.g.*, Katsube and Williamson, 1994; Vernik and Liu, 1997). Hence, although there are minor changes in porosity with increasing depth correlating approximately with the S-I transition, such changes are subtle compared with the marked change in preferred orientation.

Overpressure is commonly associated with the S-I transition. The top of the overpressure zone is normally at the same depth or slightly deeper than the top of the S-I transition zone (*e.g.*, Bruce, 1984). Disequilibrium compaction, aquathermal pressuring, and the S-I transformation are among the mechanisms proposed as the cause of overpressure as discussed, *e.g.*, by Mello *et al.* (1994). The disequilibrium compaction mechanism concerns rapid sedimentation rates that prevent fluids from readily escaping. The aquathermal mechanism requires that overpressure is generated by thermal expansion of sealed pore fluids. The S-I transformation may contribute to overpressure through the release of interlayer water into confined pore space, where porosity was diminished by textural changes caused by changes in crystallite size, orientation, and mutual boundary relations. Although there is debate on the importance of each mechanism, an effective seal must be required for each mechanism.

An ongoing TEM and XRD study of a North Sea shale sequence showing that fluid pressure increases to abnormal values, shows also the growth of illitic clay (I-S) both as a replacement of detrital phyllosilicates and in the available pore space (Nadeau *et al.*, pers. comm.). Such data are consistent with this study, which demonstrates a direct relation between the I-S transition and a change in texture that affects porosity and permeability. Geopressuring requires that the abnormally pressured fluids be sealed, and the changes in texture only provide a mechanism for sealing. However, appropriate textures in bulk shale leading to diminished porosity and permeability must be coupled with appropriate geologic structure, including a lack of fluid pathways associated, for example, with faulting. Comparison of preferred orientation in the samples described in this study with those of other sediment sequences is required to determine if the relations observed for the Gulf Coast are universal.

CONCLUSIONS

The onset of the S-I transition is intimately associated with the development of preferred orientation of phyllosilicates. The imperfect, wavy smectite layers with variable orientation relative to bedding are transformed to straight, defect-free illite packets most of which are subparallel to bedding, resulting in significant improvement in preferred orientation. The bedding-parallel orientation is consistent with development of bedding fabric in response to compaction load, resulting from dissolution-neocrystallization at smectite-illite (or I-S) boundaries and mechanical ro-

tation. The process is analogous to slaty-cleavage formation in response to elevated tectonic stress and temperature during low-grade metamorphism. These results support the proposal that coalescence of illite packets during the S-I transition provides the hydraulic seal necessary for overpressure generation. The initial development of preferred orientation at the S-I transition contributed to compaction disequilibrium, which, in turn, produced an initial condition of abnormal pressure, abnormal shale porosity, and subnormal bulk density.

ACKNOWLEDGMENTS

The single-crystal diffractometer was purchased under NSF grant EAR-8917350. This study was supported by the American Chemical Society-Petroleum Research Fund (27461-AC8) and the National Science Foundation (EAR-9614407). Special thanks are due to R. Freed (Trinity University) for providing samples and discussion. We also thank H. Dong, R. J. Merriman, and P. Nadeau for generously sharing research results, and R. Nolen-Hoeksema for discussions on physical properties of mudstones. We thank two anonymous reviewers and S. Guggenheim for their constructive, helpful reviews.

REFERENCES

Ahn, J.H. and Peacor, D.R. (1986) Transmission and analytical electron microscopy of the smectite-to-illite transition. *Clays and Clay Minerals*, **34,** 165–179.

Altaner, S.P. and Ylagen, R.F. (1997) Comparison of structural modes of mixed-layer illite/smectite and reaction mechanisms of smectite illitization. *Clays and Clay Minerals,* **45,** 517–533.

Barker, C. (1972) Aquathermal pressure—role of temperature in development of abnormal-pressure zones. *American Association of Petroleum Geologists Bulletin*, **56,** 2068–2071.

Barron, P.F., Slade, P., and Frost, R.L. (1985) Ordering of aluminum in tetrahedral sites in mixed-layer 2:1 phyllosilicates by solid-state high resolution NMR. *Physical Chemistry*, **89,** 3880–3885.

Bruce, C.H. (1984) Smectite dehydration—its relation to structural development and hydrocarbon accumulation in northern Gulf of Mexico basin. *American Association of Petroleum Geologists Bulletin*, **68,** 673–683.

Burst, J.F. (1969) Diagenesis of Gulf Coast clayey sediments and its possible relation to petroleum migration. *American Association of Petroleum Geologists Bulletin*, **53,** 73–93.

Chapman, R.E. (1980) Mechanical versus thermal cause of abnormally high pore pressures in shales. *American Association of Petroleum Geologists Bulletin*, **64,** 2179–2183.

Colten-Bradley, V.A. (1987) Role of pressure in smectite dehydration—effects on geopressure and smectite-to-illite transformation. *American Association of Petroleum Geologists Bulletin*, **71,** 1414–1427.

Dong, H. and Peacor, D.R. (1996) TEM observations of coherent stacking relations in smectite, I/S and illite of shales: Evidence for MacEwan crystallites and dominance of $2M_1$ polytypism. *Clays and Clay Minerals*, **44,** 257–275.

Dong, H., Peacor, D.R., and Freed, R.L. (1997) Phase relations among smectite, R1 illite-smectite, and illite. *American Mineralogist*, **82,** 379–391.

Freed, R.L. and Peacor, D.R. (1987) New insights on diagenesis and I/S reactions in Texas Gulf Coast sediments. *Clay Minerals*, **24,** 667–668.

Freed, R.L. and Peacor, D.R. (1989a) Geopressured shale and sealing effect of smectite to illite transition. *American Association of Petroleum Geologists Bulletin*, **73,** 1223–1232.

Freed, R.L. and Peacor, D.R. (1989b) TEM lattice fringe images with R1 ordering of illite/smectite in Gulf Coast pelitic rocks. *Geological Society of America Abstracts with Program*, **21,** A16.

Freed, R.L. and Peacor, D.R. (1992) Diagenesis and the formation of authigenic illite-rich I/S crystals in Gulf Coast shales: TEM study of clay separates. *Journal of Sedimentary Petrology*, **62,** 220–234.

Gretener, P.E. (1979) Pore pressure: Fundamentals, general ramifications, and implications for structure geology (revised). *American Association of Petroleum Geologists, Continuing Education Course Note Series 4*, 131 pp.

Guthrie, G.D., Jr. and Veblen, D.R. (1989) High-resolution transmission electron microscopy of mixed-layer illite/smectite: Computer simulation. *Clays and Clay Minerals*, **37,** 1–11.

Hower, J., Eslinger, E.V., Hower, M.E., and Perry, E.A. (1976) Mechanism of burial metamorphism of argillaceous sediment: Mineralogical and chemical evidence. *Geological Society of America Bulletin*, **87,** 725–737.

Jiang, W-T., Peacor, D.R., Merriman, R.J., and Roberts, B. (1990) Transmission and analytical electron microscopic study of mixed-layer illite-smectite formed as an apparent replacement product of diagenetic illite. *Clays and Clay Minerals*, **38,** 449–468.

Katsube, T.J. and Williamson, M.A. (1994) Effects of diagenesis on shale nano-pore structure and implications for sealing capacity. *Clay Minerals*, **29,** 451–461.

Luo, M., Baker, M.R., and LeMone, D.V. (1994) Distribution and generation of the overpressure system, Eastern Delaware Basin, Western Texas and Southern New Mexico. *American Association of Petroleum Geologists Bulletin*, **78,** 1386–1405.

Magara, K. (1975a) Reevaluation of montmorillonite dehydration as cause of abnormal pressure and hydrocarbon migration. *American Association of Petroleum Geologists Bulletin*, **59,** 292–302.

Magara, K. (1975b) Importance of aquathermal pressuring effect in Gulf Coast. *American Association of Petroleum Geologists Bulletin*, **59,** 2037–2045.

Maxwell, R.T. (1964) Influence of depth, temperature, and geologic age on porosity of quartzose sandstone. *American Association of Petroleum Geologists Bulletin*, **48,** 697–709.

Mello, U.T. and Karner, G.D. (1996) Development of sediment overpressure and its effect on thermal maturation: Application to the Gulf of Mexico Basin. *American Association of Petroleum Geologists Bulletin*, **80,** 1367–1396.

Mello, U.T., Karner, G.D., and Anderson, R.N. (1994) A physical explanation for the positioning of the depth to the top of overpressure in shale-dominated sequences in the Gulf Coast basin, United States. *Journal of Geophysical Research*, **99,** 2775–2789.

Oertel, G. (1985) The relationship of strain and preferred orientation of phyllosilicate grains in rocks—a review. *Tectonophysics*, **100,** 413–447.

Pendkar, N. and Jordan, R.R. (1993) Diagenesis of siliciclastic reservoir rocks, Baltimore Canyon Trough, Mid-Atlantic continental margin. *Geological Society of America Program with Abstracts*, **28,** A336.

Perry, E. and Hower, J. (1970) Burial diagenesis in Gulf Coast pelitic sediments. *Clays and Clay Minerals*, **18,** 165–177.

Pevear, D.R., Houser, P.J., Robinson, G.A., and Reynolds, R.C. (1997) Disorder in illite: The differences between shales, K-bentonites, and sandstones—the AFM evidence.

11th International Clay Conference, Program with Abstracts, A58.

Plumley, W.J. (1980) Abnormally high fluid pressure: Survey of some basic principles. *American Association of Petroleum Geologists Bulletin,* **64,** 414–430.

Powers, M.C. (1967) Fluid-release mechanisms in compacting marine mudrock and their importance in oil exploration. *American Association of Petroleum Geologists Bulletin,* **51,** 1240–1254.

Reynolds, R.C., Jr. (1992) X-ray diffraction studies of illite/smectite from rocks, <1 μm randomly oriented powders and <1 μm oriented powder aggregates: The absence of laboratory-induced artifacts. *Clays and Clay Minerals*, **40,** 387–396.

Sharp, J.M., Jr. (1983) Permeability controls on aquathermal pressuring. *American Association of Petroleum Geologists Bulletin*, **67,** 2057–2061.

Sintubin, M. (1994) Clay fabric in relation to the burial history of shales. *Sedimentology*, **41,** 1161–1169.

Srodon, J. (1980) Precise identification of illite/smectite interstratifications by X-ray powder diffraction. *Clays and Clay Minerals*, **32,** 337–349.

van der Pluijm, B.A., Ho, N-C., and Peacor, D.R. (1994) High-resolution X-ray texture goniometry. *Journal of Structural Geology*, **16,** 1029–1032.

van der Pluijm, B.A., Ho, N-C., and Peacor, D.R. (1995) High-resolution X-ray texture goniometry: Reply. *Journal of Structural Geology*, **17,** 925–926.

van der Pluijm, B.A., Ho, N-C., Merriman, R.J., and Peacor, D.R. (1998) Contradictions of slate formation resolved? *Nature*, **392,** 348.

Velde, B., Suzuki, T., and Nicor, E. (1986) Pressure-temperature-composition of illite/smectite mixed-layer minerals: Niger Delta mudstones and other examples. *Clays and Clay Minerals*, **34,** 435–441.

Vernik, L. and Liu, X. (1997) Velocity anisotropy in shales: A petrophysical study. *Geophysics*, **62,** 521–532.

Wenk, H-R. (1985) Measurement of pole figures. In *Preferred Orientation in Deformed Metals and Rocks: An Introduction to Modern Texture Analysis*, H.R. Wenk, ed., Academic Press, New York, 11–47.

(Received 18 February 1998; accepted 18 February 1999, Ms. 98-027)